Multi-UAV active sensing for precision agriculture via Bayesian fusion

Luca Pierdicca[1], Dimitri Ognibene[2] and Vito Trianni[1]

***Abstract*— Unmanned aerial vehicles (UAVs) represent a well established technology for the monitoring and mapping of crop fields in precision agriculture applications. In order to fully exploit all the possibilities they offer, a key challenge is devising optimal flight plans that maximize both data accuracy and field coverage. Active sensing techniques have shown promising results in this direction, as they permit online adaptation of plans based on the monitoring objective at hand. Here, we propose an active sensing strategy for multiple autonomous UAVs based on the concept of information gain, and a factor graph field representation for mapping in a Bayesian framework by taking into account spatial correlation effects. We validate our approach on a simulated feature detection scenario, and study the effects of different feature distributions and varying levels of information sharing. Simulation results show large performance improvements over common non adaptive methods based on uniform or random-walk monitoring, highlighting the advantages of active monitoring in reducing uncertainty and maximizing coverage.**

I. INTRODUCTION

Precision agriculture relies on the use of accurate data about crop health and growth to define the best management strategies and adopt solutions targeted at the individual plant [1]. To obtain increasingly accurate data, more and more advanced technological solutions are making their way into the national and international market. Without doubt, UAVs represent a well established technology as they enable flying over a field and collect detailed images to be analyzed for a wide variety of purposes [2], [3]. Despite the proliferation of drone service providers, the real utility of the collected data is nowadays limited to the detection of generic indices (e.g., the NDVI index of vegetation), and the unexpressed potential of drones remains very high. The reasons behind these limitations are associated with the demand for high levels of detail to enable advanced AI feature detection methods and the limited flight times offered by commercially available drones.

To obtain relevant information (e.g., the level of fruit ripening or the occurrence of a disease on a plant), it is necessary to observe plants frequently and with a high resolution. Close-up images obtained from multiple perspectives can be used to generate three-dimensional representations of the plant, and they can also be analyzed by appropriately trained computer vision algorithms, providing surprisingly accurate results [4]. In order for a drone to obtain images at the desired level of detail, it must be able to get close enough (depending on the quality of the available optical sensor) by flying at low altitude. However, flying at low altitude poses two problems: (i) it brings limitations on the speed of flight to obtain sharp images, and (ii) it allows only small portions of the field to be observed at each instant. The first point limits the use of fixed-wing drones, capable of flying for long periods but at a relatively high cruising speed, thus forcing the use of rotary-wing drones. The second point requires a higher observation time for large fields, clashing with typical battery lifetimes for drones, which are limited to a few dozens of minutes of flight time. Monitoring a field at a sufficient level of detail would require many consecutive missions and associated battery replacements, making operations more time-consuming and expensive.

In order to overcome these limitations, it is necessary to abandon the usage of UAVs as passive sensing devices, and to exploit the autonomy of drones to actively determine where and when to perform an observation of the field [5]. In other words, by means of an "active sensing" approach, autonomous UAVs can recognize relevant features and adapt the flight plan (trajectory, altitude) to specific monitoring needs, obtaining multiple-resolution images and from different perspectives to allow for 3D reconstruction and greater accuracy in classifying points of interest (POIs), i.e., areas, plants or parts of them judged to be of relevance to a specific agronomic objective. Whatever the monitoring objective, an active sensing approach makes it possible to take full advantage of the UAV's ability to move through space and hover over a POI, while at the same time allowing an optimal flight plan to be defined to maximize both data accuracy and complete field coverage. In addition, groups of UAVs can coordinate and collaborate with each other for active sensing, while increasing efficiency—thanks to the parallelization of operations—and accuracy—thanks to the collaboration between drones.

Active sensing is based on two intertwined processes. First, UAVs maintain and update an internal world model, that is, a representation of the field as a map. Second, UAVs perform online planning exploiting the internal world model to maximise a given performance metric [6], [7]. Various approaches have been proposed for field mapping. An occupancy grid approach discretises the field in a grid of cells which are usually updated independently one from the other [8], [9], [10]. This conventional approach does not capture spatial correlations in the distribution of POIs,

VT acknowledges support from the project E-CROPS (Technologies for Digital and Sustainable Agriculture, funded by the Italian Ministry of University and Research, Contract ARS01_01136) and from the project AGR-o-RAMA (Active monitoring for Agricultural Robots, POR FESR Lazio 2014-2020, Grant Agreement B85F21001360006).

[1]Luca Pierdicca and Vito Trianni are with the Institute of Cognitive Sciences and Technologies, National Research Council, Rome, Italy; vito.trianni@istc.cnr.it

[2]Dimitri Ognibene is with the BiConnect, Center for Human Technology Connection Research, Università Milano-Bicocca dimitri.ognibene@unimib.it

which are however very common in the real world. A different approach consists in employing Gaussian Processes to capture the heterogeneity of a field [11], [12], [13]. This also enables to build maps at multiple resolutions, in which areas with high density of POIs are mapped at a higher resolution than areas devoid of POIs [14], [15]. ND-tree structures (e.g., quad-trees) can be exploited to build maps at different resolutions, where some branches of the tree develop at larger depths [16], [17]. Finally, several approaches represent the field as a semantic map, where different areas are assigned a label, often resulting from deep learning methods [18], [19]. Both multi-resolution methods and semantic maps depend on the accuracy of the sensor, which highly depends on the distance from the POIs [20]. In the case of UAVs flying over a field, the relevant parameters is the altitude: the higher the UAV flies, the lower the sensor accuracy. For instance, increasing the altitude leads to higher ground sample distances, that is, the distance on the ground between two adjacent pixels increases linearly with the altitude. This has a negative effect on the accuracy of any vision model [21], and consequently of the generated map. Accuracy reduction can be concealed with adaptive planning approaches (i.e., informative path planning), which exploit information gathered from the field to define the best observation sequence. Adaptive planning improves over offline planning approaches [10], [14] thanks to the possibility of adapting the sampling frequency or resolution as a function of the mapping requirements. Several approaches can be exploited, for instance receding horizon planners [22], Monte-Carlo tree search approaches [23], optimisation-based strategies [24], [10] and geometric approaches [19]. Such approaches have in common the possibility to observe the same region multiple times—possibly varying altitude—to reduce the uncertainty in the feature detection and improve the map accuracy. Planning in this case takes into account information theoretic measures such as the Information Gain, that is, the expected reduction of uncertainty from a further observation. Also, the posterior reduction of uncertainty can be used as a signal for reinforcement learning approaches [25], [26]. Finally, multi-UAV approaches have been proposed as well, whereby different UAVs contribute to map a large field, either by partitioning it in multiple non-overlapping areas, or by collaborating and focusing on the regions of highest interest [27], [28]. However, challenges related to real-world deployment must be considered, such as asynchronous decision making and limitations in communication range and bandwidth [29].

In this study, we propose a novel active sensing approach for multiple autonomous UAVs, whereby the mapping is based on the occupancy-grid approach, but takes into account spatial correlations by means of a field representation that exploits a factor graph. To compute the posterior marginals after an observation, we exploit the Loopy Belief Propagation approach, which enables to diffuse information to neighbouring cells of the grids according to predefined correlation weights. Given that multiple UAVs contribute to the mapping effort, individual beliefs are shared with neighbours and fused with the internal world model, leading to better informed planning. The latter is based on the maximisation of the Information Gain, and accounts for (i) observations at multiple altitudes and (ii) increased efficiency of group behaviour. We show that the proposed approach largely improves over common baseline approaches based on pre-planned uniform monitoring or on random-walk approaches, suggesting that active monitoring is beneficial for quickly reducing uncertainty while maximising coverage. Additionally, we show that spatial correlations can be effectively exploited to improve the mapping efficiency, and that an adaptive approach that links the relevance of correlations to the obtained observations better trades off between speed and accuracy when the amount of spatial correlation in the field is a priori unknown. Finally, we demonstrate how sharing information among UAVs largely improves performance and convergence of the individual world models to a shared representation.

The paper is organised as follows. Section II formally introduces the mapping problem and the devised solutions. Section III-A discussed simulation results for both single and multi-UAV experiments. Section IV concludes the paper with some discussion and future perspectives.

II. Problem Statement

We consider an active field-monitoring task employing a team of UAVs. The goal is to plan paths for efficient data collection to identify regions where interesting features appear. In order to assess the effectiveness of the proposed methodology, we exploit a simulated scenario for feature detection on synthetic terrains.

A. Simulated environment

The environment is based on a grid-world simulator where the terrain is represented as a set of equally sized square cells, while the agent configuration space is discretised into a 3D lattice. We assume perfectly known UAV position and finite action spaces. Moreover, we equip each UAV with a downward facing sensor allowing for measurements of features within a squared patch of the field.

As a UAV moves above the terrain, observations are collected and fused into a local terrain belief, representing the estimated probability of occupancy (e.g., weed presence) for each cell. To foster coordination, UAVs can share their position and local beliefs broadcasting the information to neighbor UAVs within their communication range.

B. Sensor Model

Depending on the position, UAVs can observe variable size patches of the field, referred to as footprints—the higher the altitude, the larger the footprint size. We denote the footprint bounding box associated to a position $\boldsymbol{x}$ as $fp(\boldsymbol{x})$ and the subset of terrain cells within the footprint bounding box as $\mathcal{C}(\boldsymbol{x})$. Given the position of a UAV and assuming a squared footprint, $fp(\boldsymbol{x})$ and $\mathcal{C}(\boldsymbol{x})$ can be computed exploiting the following relation:

$$d(h) = 2h \tan\left(\frac{FoV}{2}\right) \tag{1}$$

where d is the side of the footprint bounding box, h is the UAV altitude and FoV is the camera field-of-view angle.

In order to model the increasing noise and ground sampling distance in high-altitude observations, similar to [10], we leverage a position-dependent probabilistic sensor model:

$$p(z|m,\boldsymbol{x}) = \begin{cases} 1-\sigma(\boldsymbol{x}) & \text{if } z = m \\ \sigma(\boldsymbol{x}) & \text{if } z \neq m \end{cases} \tag{2}$$

where $m \in \{0,1\}$ is the cell state, $z \in \{0,1\}$ is the measurement of the cell state, $\boldsymbol{x} \in \mathbb{R}^3$ is the UAV position and $\sigma \in [0,1]$ expresses false positives and false negatives rates, profiling higher rates as altitude increases:

$$\sigma(h) = a\,\left(1 - e^{-bh}\right) \quad \text{with } a, b > 0 \tag{3}$$

Note that error rates are limited to $\sigma = 0.5$, corresponding to a sensor that does not provide any information about a cell. We report some examples of σ profiles in Fig. 1-Left.

C. Terrain Mapping

Mapping is formulated as a probabilistic estimation problem of the terrain state which is assumed global and static. In detail, each terrain cell is associated with a binary random variable m encoding the presence of relevant features. Noisy cell measurements $\boldsymbol{z}$, gathered by UAVs for every cell within their footprints, are fused into a local terrain belief $\mathcal{B}$ at each step, in a recursive Bayesian fashion.

In order to capture spatial correlations which typically arise in natural phenomena, we exploit the flexibility of undirected graphical models. In particular, we model the feature distribution through a pairwise Conditional Random Field (CRF). Formally, the CRF is described by a grid-like undirected graph which represents a conditional probability distribution over hidden and observed variables $\mathcal{M} \cup \mathcal{S}$ as a product of factors:

$$p(\boldsymbol{m}|\boldsymbol{s}) = \frac{1}{Z(\boldsymbol{s})} \prod_{i=1}^{k} \phi_e(m_i, \boldsymbol{o}) \prod_{\substack{i,j \in \{1,\dots,k\} \\ (i,j) \in E}} \phi_p(m_i, m_j, \boldsymbol{o}) \tag{4}$$

where we interpret $\boldsymbol{m} = (m_1, \dots, m_n) \in \mathcal{M}$ as the set of terrain cells and $\boldsymbol{s} = (\boldsymbol{o}_1, \dots, \boldsymbol{o}_T) \in \mathcal{S}$ as the history of observations with elements $\boldsymbol{o}_t = (\boldsymbol{x}_t, z_{t,1}, \dots, z_{t,k})$ including both the UAV position $\boldsymbol{x}_t$ and the measurements $\boldsymbol{z}_t$ of the cells $m_i \in \mathcal{C}(\boldsymbol{x}_t)$ with $k = |\mathcal{C}(\boldsymbol{x}_t)|$. $Z(\boldsymbol{s})$ is known as the partition function (a normalizing term) and $\phi_e(m_i, \boldsymbol{o})$, $\phi_p(m_i, m_j, \boldsymbol{o})$ are generic non-negative functions of the cell state m_i and the last observation $\boldsymbol{o}$. For notation parsimony, we dropped the time t index in Equation (4), however all products involve both space and time. Evidence factors such as ϕ_e are associated to the set of nodes V of the graph and are used to model interactions between observed and hidden variables, whereas pairwise factors like ϕ_p are associated to the set of edges E of the graph and are used to model interactions between the hidden variables. We define the factors as follows:

$$\phi_e(m_i, \boldsymbol{o}) = p(z_i|m_i, \boldsymbol{x}) \tag{5}$$

$$\phi_p(m_i, m_j, \boldsymbol{o}) = w_{m_i,m_j}(\boldsymbol{o}) \tag{6}$$

where the weights $w_{m_i,m_j}(\boldsymbol{o})$ encode the strength of the spatial correlations.

The mapping inference task is to compute the posterior *marginals* $p^+(m_i) = p(m_i|\boldsymbol{o}_{1:t})$ for all cells $m_i \in \mathcal{C}(\boldsymbol{x}_t)$ at each step, as a new observation $\boldsymbol{o}_t$ is collected, exploiting Bayesian recursive updates that involve prior marginals and observation likelihoods. To this end, we exploit the Sum-Product variant of the Loop Belief Propagation (LBP) algorithm [30].

D. Planning

The policy adopted by the UAVs consists in choosing the action $a \in \mathcal{A}(\boldsymbol{x}_t) \subseteq \boldsymbol{A}$ that maximizes the information gain (i.e., the expected uncertainty reduction) of $\mathcal{B}$, over a one-step horizon [27]. We use $\boldsymbol{A} = \{\text{up}, \text{down}, \text{front}, \text{back}, \text{left}, \text{right}, \text{hover}\}$, in which, depending on $\boldsymbol{x}_t$, we do not consider actions that exceed the limits of the UAV configuration space. To compute the information gain, we simulate a terrain belief Bayes update at each step leveraging on the posterior marginals, that we interpret here as cells priors, and a candidate observation (i.e., an observation that we average over). In greater details, on the basis of the available information about a cell m_i at time t, it is possible to compute the Information Gain $IG(m_i, \hat{\boldsymbol{x}}_{t+1})$ as the difference between the cell entropy at time t—i.e., the entropy of the prior distribution of a cell—and the cell entropy conditioned on the possible observations $\hat{\boldsymbol{o}}_{t+1}$ from a candidate position $\hat{\boldsymbol{x}}_{t+1}$—i.e., the *expected* entropy of the posterior distribution of a cell:

$$IG(m_i, \hat{\boldsymbol{x}}_{t+1}) = H(m_i) - H(m_i|\hat{\boldsymbol{o}}_{t+1}), \tag{7}$$

where we have that

$$H(m_i) = -\sum_{m_i} p^-(m_i) \log(\, p^-(m_i)\,),$$

$$H(m_i|\hat{\boldsymbol{o}}_{t+1}) = \sum_{\hat{z}_{t+1,i}} p(\hat{\boldsymbol{o}}_{t+1}) \big[-\sum_{m_i} p^+(m_i) \log(\, p^+(m_i)\,) \big]$$

and

$$p^-(m_i) = p(m_i \mid z_{0:t,i}, \boldsymbol{x}_{0:t}),$$

$$p(\hat{\boldsymbol{o}}_{t+1}) = p(\hat{z}_{t+1,i}, \hat{\boldsymbol{x}}_{t+1}),$$

$$p^+(m_i) = p(m_i \mid z_{0:t,i}, \boldsymbol{x}_{0:t}, \hat{z}_{t+1,i}, \hat{\boldsymbol{x}}_{t+1})$$

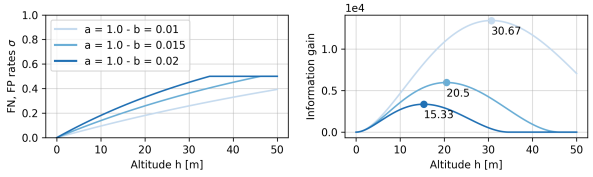

Fig. 1. Altitude dependent probabilistic sensor model. Left: example false negatives and false positives curves. Right: variation of the information gain $IG(\boldsymbol{x}) = \sum_{m_i \in \mathcal{C}(\boldsymbol{x})} IG(m_i, \boldsymbol{x})$, where $\boldsymbol{x} = [0, 0, h]$ with $h \in [0, 50]$ and constant, maximum uncertainty for $\mathcal{B}$. Maximum values are reported as dots. Larger σ increasing rates lead to lower optimal altitudes.

Regarding planning, given the current agent position $\boldsymbol{x}_t$, we evaluate each valid action $a \in \mathcal{A}(\boldsymbol{x}_t)$ based on the associated information gain. Considering $\hat{\boldsymbol{x}}_{t+1}$ to be the position that would be reached executing a, we define IG_a as the sum of the information gain of the cells within the footprint $\mathcal{C}(\hat{\boldsymbol{x}}_{t+1})$:

$$IG_a = \sum_{m_i \in \mathcal{C}(\hat{\boldsymbol{x}}_{t+1})} IG(m_i, \hat{\boldsymbol{x}}_{t+1}) \tag{8}$$

and the final action selection can be stated as

$$a^* = \arg\max_{a \in \mathcal{A}(\boldsymbol{x}_t)} IG_a \tag{9}$$

Note that the choice of an action depends both on the number of cells that are covered by the footprint, and by the altitude at which the observation is performed. Indeed, by increasing the altitude, the footprint becomes larger, meaning that more cells are summed up into the calculation of IG_a. At the same time, the error rates increase, reducing the average information gain per cell. The right panel in Fig. 1 shows how the IG varies with the altitude h starting with maximum uncertainty for $\mathcal{B}$. It is possible to notice that there exist an optimal altitude at which the information gain is maximised. In multi-agent scenarios, where multiple UAVs are deciding in parallel, we simulate asynchronous decisions by updating a single agent at a time and randomising the order of updates.

E. Information Sharing

To achieve coordinated agent behavior, UAVs can exploit communication to share information about their positions and about their local beliefs.

1) Position: To discourage interference among UAVs, we apply to IG_a a discount factor that takes indirectly into account the distance between the agents. Leveraging on their footprints, we define the discount factor $\alpha^{ij} \in [0, 1]$ between agents i and j as the intersection over union (IoU) of their footprints:

$$\alpha^{ij} = 1 - IoU(fp(\boldsymbol{x}^i), fp(\boldsymbol{x}^j)) \tag{10}$$

and the discounted IG_a for agent i with neighborhood $\mathcal{N}$ as

$$IG_{ad} = IG_a \prod_{j \in \mathcal{N}} \alpha^{ij} \tag{11}$$

In greater detail, each agent performs the following steps:

1) simulate the execution of all admissible actions and compute their IG_a
2) from its original position, retrieve the position of its neighbors (assuming that successive agents in the order of updates are static) and compute IG_{ad}
3) execute the best action, and move to the new position (the planned position)

Note that in the second step, depending on the order of updates, all the previous agents have already moved to their planned position. This scheme ensures that subsequent agents action selection will be influenced by the previously selected agents actions.

The factor α^{ij} penalizes actions that make footprints overlap, taking into account the altitude of the agents. Indeed, assuming equal overlaps (i.e., intersection), footprints at lower altitudes produce larger penalization values (due to smaller union) than footprint at higher altitudes. Hence, α^{ij} captures implicitly the intuition that simultaneous low-altitude high-precision and high-altitude low-precision observations of a subset of cells should be discouraged.

2) Belief: Alignment of local terrain beliefs among UAVs is achieved by sharing private information and fusing received data into the own belief. To this end, each UAV maintains a separate representation of the world that encodes solely the most recent observations from the last time information was shared. We call this world representation "news belief" $\hat{\mathcal{B}}$. By sharing only the encoded news (the news belief) rather than the encoding of the entire history of observations (the terrain belief), the phenomenon of double counting can be avoided and the final fusion between terrain and news beliefs can be realized, on the receiver side, through simple re-normalisation of beliefs. Moreover, to limit the loss of information, each UAV i can store and maintain multiple news beliefs $\hat{\mathcal{B}}_j$, one for each agent $j \neq i$, at the expense of an increased memory requirement.

III. Experimental Results

We validate our approach in a simulated feature detection scenario performing several experiments where we generate synthetic correlated Gaussian random field terrains parameterized by their cluster radius value (Fig. 2). We consider terrains of size $50\,\mathrm{m} \times 50\,\mathrm{m}$, discretised into cells with resolution $c_r = 12.5\,\mathrm{cm}$ (i.e., 400×400 cells). Also, we use a discretised configuration space with horizontal resolution of ~ 3 m for a total of 17 way-points per side, and a vertical resolution of ~ 5.4 m for a total of 6 altitudes, from ~ 5.4 m to ~ 32.4 m. We set the camera $FoV = \frac{\pi}{3}$ to guarantee, for every altitude, the existence of observation points from which the footprint does not exceed the monitored area near corners and boundaries. Should the camera footprint exceed the monitored area, any parts of the image that fall outside would be ignored. We set the sensor model parameters to a = 1 and b = 0.015 (see left panel in Fig. 1). The associated false positives and false negatives rates σ for each altitude are $\{0.07, 0.15, 0.22, 0.28, 0.33, 0.40\}$. We consider experimental conditions with terrain cluster radius $r \in \{0, 1, 2, 3, 4, 5\}$, team size $N \in \{1, 2, 4, 8\}$ and communication range $R \in \{5\,\mathrm{m}, \infty\}$. In multi-agent settings, we report results for different levels of information sharing.

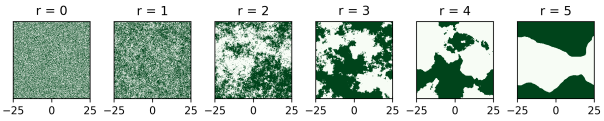

Fig. 2. Example of synthetic Gaussian random field terrains with increasing value of cluster radius r. Higher values of r correspond to highly correlated terrains with larger clusters, whereas values near zero correspond to terrains with a random feature distribution

We define three different approaches for the pairwise factor weights $w_{m_i,m_j}(\boldsymbol{o})$, referred to as "equal", "biased" and "adaptive". The first two use fixed values, defined as follows:

$$\begin{aligned} \text{equal} &:= w_{m_i,m_j}(\boldsymbol{o}) = 0.5 \;\forall\; m_i, m_j \in \{0,1\} \\ \text{biased} &:= w_{m_i,m_j}(\boldsymbol{o}) = 0.7 \text{ if } m_i = m_j, \\ & \quad\; w_{m_i,m_j}(\boldsymbol{o}) = 0.3 \text{ if } m_i \neq m_j \end{aligned}$$

Equal weights ignore any relation between the cells whereas biased weights promote locally coherent cell values by taking into account spatial interactions. Lastly, the adaptive approach varies the weights according to the experienced contingency, hence trying to adapt to the current observation. Precisely, the adaptive weights are obtained by the sample estimate of the Pearson correlation coefficient $\hat{\rho}_{c,n}$ between variables c and n normalized through a sigmoid function. We consider non overlapping Von Neumann neighborhoods of $\boldsymbol{z}$, and we define the random variables $c \in \{0,1\}$ to be the value of the central cell and $n \in \{0,1,2,3,4\}$ to be the total number of positive values in its four adjacent cells. We collect the sample set $\mathcal{D} = \{(c_1,n_1),\ldots,(c_h,n_h)\}$ with size $h = |\mathcal{C}(\boldsymbol{x})|/9$. Finally, we set the adaptive weights as follows:

$$\begin{aligned} \text{adaptive} &:= w_{m_i,m_j}(z) = \frac{1}{1+e^{-\hat{\rho}_{c,n}}} \text{ if } m_i = m_j, \\ & \quad\; w_{m_i,m_j}(z) = \frac{e^{-\hat{\rho}_{c,n}}}{1+e^{-\hat{\rho}_{c,n}}} \text{ if } m_i \neq m_j \end{aligned}$$

where

$$\hat{\rho}_{c,n} = \frac{\sum_{i=1}^{h}(c_i-\bar{c})(n_i-\bar{n})}{\sqrt{\sum_{i=1}^{h}(c_i-\bar{c})^2}\sqrt{\sum_{i=1}^{h}(n_i-\bar{n})^2}}$$

Here, $\bar{c}$ and $\bar{n}$ are the average over $\mathcal{D}$. Overall, weights converge to 0.5 when correlation is low, otherwise they are the more biased the higher is the correlation coefficient.

In the following, for each experimental condition we perform 20 repetitions with random terrains and maximum initial uncertainty in $\mathcal{B}$. To evaluate the performance we consider the evolution of two metrics over time: the total entropy of the whole terrain belief and the mean squared error between the terrain belief and the true terrain, averaged over all repetitions of the experiments and over all UAVs.

A. Comparison against baseline planners

In this set of experiments, we deploy a single agent in the field and we compare our planning strategy ("IG") against two baseline planners: (i) a stochastic exploration strategy where actions are sampled uniformly at random (referred to as "Random"); (ii) a lawnmower strategy performed at the optimal altitude (referred to as "Sweep"). Here, the optimal altitude is set at $h = 21.65$, which is the allowed value closest to the altitude that maximises the information gain as shown in Fig. 1 right.

We set $w = equal$ assuming independence between the cells. In all experiments, we generate random terrains with cluster radius $r = 5$ and we set the UAV initial position in the lower left corner of the terrain at the minimum altitude.

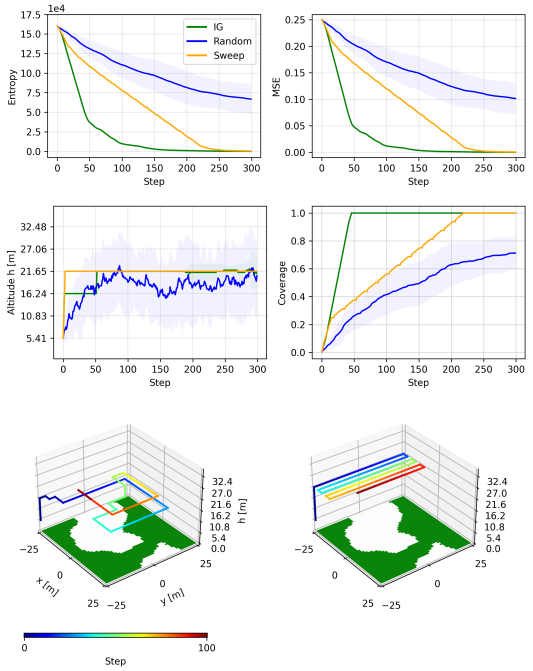

Fig. 3. Comparison of planning strategies for $N = 1$, $r = 5$ and $w = equal$. Top: entropy and MSE evolution of the terrain belief. Center: UAV altitude and coverage evolution. Shaded areas represent standard deviations, and the solid lines indicate means over 20 runs. Bottom: example trajectories for our planning strategy "IG" (left) and the baseline strategy "Sweep" (right). Paths are limited to 100 steps.

In the Sweep strategy, the UAV first moves to the optimal altitude and then starts sweeping over the field.

Fig. 3-Top shows the evolution of the evaluation metrics for all planners. As expected, IG leads to faster entropy and MSE reduction rates with respect to the other planning strategies. This is because IG permits adaptive position selection based on the current knowledge of the terrain $\mathcal{B}$, trading off quality and quantity of observations. Specifically, decreasing rates are faster during the first 50 steps of the mission, when the UAV observes the whole field for the first time at $h = 16.24$ (Fig. 3-Center), then, as it reaches the optimal altitude, IG starts tracing a square shaped trajectory, which efficiently minimize the overlap between footprints, promoting exploration towards unobserved or less frequently observed regions (e.g., the field corners) and simultaneously avoid footprint cropping along the borders and corners (Fig. 3-Bottom). This is in contrast to the other strategies, in fact, the Sweep strategy constrains the UAV to a uniform non-adaptive and linear scanning of the terrain causing constant decreasing rates, whereas the Random strategy, by selecting the next action uniformly at random, leads to inefficient exploration and poor performance.

B. Varying pairwise factor weights for mapping

In this section, we consider only the IG planning strategy and we systematically investigate the effect on performance of varying pairwise factor weights for mapping and varying terrain cluster radius. We deploy a single agent

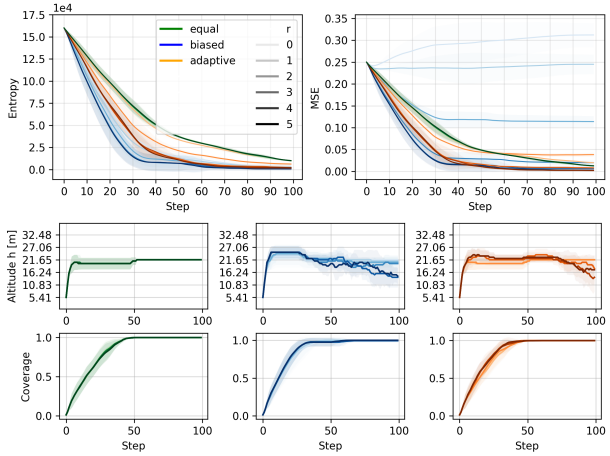

Fig. 4. Effect of varying factor weights w and cluster radius r for our planner IG with $N = 1$. Top: entropy and MSE evolutions for the considered r and w. Bottom: UAV altitude and coverage evolution. Darker shades correspond to higher values of r. Shaded areas represent standard deviations, and the solid lines indicate means over 20 runs.

in the field and we set $r = \{0, 1, 2, 3, 4, 5\}$ and $w = \{equal,\ biased,\ adaptive\}$.

The top panels of Fig. 4 show that when $w = equal$ the performance is not dependent on the cluster radius value, whereas when $w = biased$, the performance is particularly sensitive to it. Specifically, when $w = biased$ and $r = \{3, 4, 5\}$, the error becomes negligible as soon as the field is fully covered, which is a major improvement compared to $w = equal$. When $r = \{0, 1, 2\}$, the error exhibits increasing trends or premature convergence. Such performance variations are attributed to the discrepancy between assumed and actual terrain correlation levels. In other words, the biased approach assumes correlations between adjacent cells in the field, which are not present when $r \leq 2$.

To mitigate this effect, we can employ adaptive weights by estimating the correlation level based on a collected measurement. As depicted in Fig. 4-Right, this approach yields a good compromise when the terrain is not known a priori and demonstrates overall satisfactory results in most cases, despite being solely based on estimates from very limited and spatially heterogeneous samples (i.e., single measurements). In fact, we still encounter premature convergence of the error when $r = 2$. We can hypothesize that this is due to both the noise present in the observations, which compromises reliable estimation of the correlation level, and the altitude from which the observations are collected. Indeed, lower altitudes are associated with smaller size observation areas, which in this case could lead to an overestimation of the correlation level. Nevertheless, we can see that we are able to reproduce behaviors that are similar to those obtained in non adaptive weights setups (see Fig. 4-Bottom). Specifically, we observe that agents tend to fly at lower altitude towards the end of a mission when $r >= 3$. This is due to the presence of smoother clusters boundaries in that kind of terrains. These boundaries represent the most challenging area to classify when $w = biased$. Consequently, agents tend to adapt their

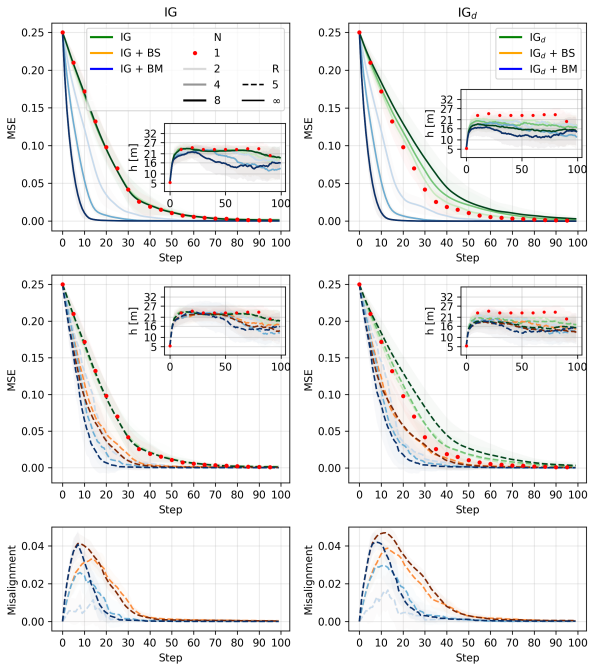

Fig. 5. Effect of information sharing in multi-agent scenarios for our planning strategies (IG - left column and IG$_d$ - right column). Top: MSE evolution for $R = \infty$. Center: MSE evolution for $R = 5$. Bottom: local beliefs misalignment evolution. Shaded areas represent standard deviations, and solid or dashed lines indicate means over 20 runs. Given that some experimental setups lead to equivalent results (e.g., BM and BS with $R = \infty$) the corresponding curves overlap and are not all visible.

altitude, focusing on the cells where uncertainty is larger, to attain higher precision measurements.

C. Effect of information sharing

Next, we perform experiments in multi-agent scenarios with different levels of information sharing. In particular, we set $N = \{2, 4, 8\}$, $w = adaptive$, $r = 5$ and $R = \{5, \infty\}$. In all scenarios, we set random initial positions for the UAVs. We compare our planning strategy ("IG")—no information sharing—and its discounted variant ("IG$_d$")—with position sharing—when (i) a single news belief is shared and fused into the neighbors local beliefs ("BS"); (ii) private per-agent news beliefs are shared and fused into the neighbors local beliefs ("BM").

From the top panels in Fig. 5, a significant performance improvement can be noted as the level of shared information among agents increases. Indeed, at the expense of larger memory requirements, leveraging private sharing channels (BM), as opposed to a single sharing channel (BS), permits the accumulation of longer and more specialized observation histories, as private news beliefs are reset less frequently. Also, a limited communication range ($R = 5$) leads to slower mapping dynamics, as expected due to the higher misalignment of the individual maps (middle panels in Fig. 5).

Somewhat surprisingly, by comparing the two planning strategies (Fig. 5 top-left and top-right), we can see that the effect of discounting the information gain is counterproductive in some cases. Essentially, IG$_d$ fosters larger inter-agents

distances and also promotes lower altitudes (see insets in Fig. 5). In scenarios where belief sharing is not active, for any R and N, performance decreases (green curves). Whereas, when belief sharing is active, performance drop is somewhat compensated for, but to a lower extent when $R = 5$. In the latter case, it takes longer to UAVs to align their beliefs (see Fig. 5 bottom). Overall, action discounting leads to larger misalignment and slower convergence rates.

IV. Conclusions

In this paper, we introduced an active sensing technique based on information gain. Results from simulations of a field-monitoring task with a single agent showed a significant performance increase compared to non-adaptive approaches. Additionally, we demonstrated the benefits of using a factor graph based mapping technique, capable to adapt spatial correlation effects across different terrain types. Finally, we illustrated how further performance improvements can be achieved in multi-agent scenarios by examining the impact of information sharing at various levels. Future directions will focus on exploring potential extensions of the informed planning criterion to enhance coordination, incorporating neighborhood terrain knowledge instead of relying on distance-based heuristics. Moreover, we will investigate the integration of our approach into a fully Bayesian framework, wherein model parameters are learned during mapping. Finally, we will address real-world monitoring tasks.

References

[1] R. Gebbers and V. I. Adamchuk, "Precision Agriculture and Food Security," *Science*, vol. 327, no. 5967, pp. 828–831, 2010.

[2] C. Zhang and J. M. Kovacs, "The application of small unmanned aerial systems for precision agriculture: a review," *Precision Agriculture*, vol. 13, no. 6, pp. 693–712, 2012.

[3] S. K. Phang, T. H. A. Chiang, A. Happonen, and M. M. L. Chang, "From satellite to uav-based remote sensing: A review on precision agriculture," *IEEE Access*, vol. 11, pp. 127 057–127 076, 2023.

[4] J. Su, X. Zhu, S. Li, and W.-H. Chen, "Ai meets uavs: A survey on ai empowered uav perception systems for precision agriculture," *Neurocomputing*, vol. 518, pp. 242–270, 2023.

[5] T. Veiga and J. Renoux, "From Reactive to Active Sensing: A Survey on Information Gathering in Decision-theoretic Planning," *ACM Computing Surveys*, vol. 55, no. 13s, pp. 1–22, 2023.

[6] D. S. Chaplot, D. Gandhi, S. Gupta, A. Gupta, and R. Salakhutdinov, "Learning to explore using active neural slam," *arXiv preprint arXiv:2004.05155*, 2020.

[7] T. Taniguchi, S. Murata, M. Suzuki, D. Ognibene, P. Lanillos, E. Ugur, L. Jamone, T. Nakamura, A. Ciria, B. Lara, *et al.*, "World models and predictive coding for cognitive and developmental robotics: frontiers and challenges," *Advanced Robotics*, vol. 37, no. 13, pp. 780–806, 2023.

[8] A. Elfes, "Using occupancy grids for mobile robot perception and navigation," *Computer*, vol. 22, no. 6, pp. 46–57, 1989.

[9] B. Charrow, S. Liu, V. Kumar, and N. Michael, "Information-theoretic mapping using cauchy-schwarz quadratic mutual information," in *2015 IEEE International Conference on Robotics and Automation (ICRA)*, 2015, pp. 4791–4798.

[10] M. Popović, T. Vidal-Calleja, G. Hitz, J. J. Chung, I. Sa, R. Siegwart, and J. Nieto, "An informative path planning framework for uav-based terrain monitoring," *Autonomous Robots*, vol. 44, pp. 889–911, 2020.

[11] S. Vasudevan, F. Ramos, E. Nettleton, and H. Durrant-Whyte, "Gaussian process modeling of large-scale terrain," *Journal of Field Robotics*, vol. 26, no. 10, pp. 812–840, 2009.

[12] S. T. O'Callaghan and F. T. Ramos, "Gaussian process occupancy maps," *The International Journal of Robotics Research*, vol. 31, no. 1, pp. 42–62, 2012.

[13] A. Reid, F. Ramos, and S. Sukkarieh, "Multi-class classification of vegetation in natural environments using an unmanned aerial system," in *2011 IEEE International Conference on Robotics and Automation*, 2011, pp. 2953–2959.

[14] L. Jin, J. Rückin, S. H. Kiss, T. Vidal-Calleja, and M. Popović, "Adaptive-resolution field mapping using gaussian process fusion with integral kernels," *IEEE Robotics and Automation Letters*, vol. 7, no. 3, pp. 7471–7478, 2022.

[15] F. Stache, J. Westheider, F. Magistri, C. Stachniss, and M. Popović, "Adaptive path planning for UAVs for multi-resolution semantic segmentation," *Robotics and Autonomous Systems*, vol. 159, p. 104288, 2023.

[16] A. Hornung, K. M. Wurm, M. Bennewitz, C. Stachniss, and W. Burgard, "OctoMap: an efficient probabilistic 3D mapping framework based on octrees," *Autonomous Robots*, vol. 34, no. 3, pp. 189–206, 2013.

[17] N. Funk, J. Tarrio, S. Papatheodorou, M. Popović, P. F. Alcantarilla, and S. Leutenegger, "Multi-resolution 3d mapping with explicit free space representation for fast and accurate mobile robot motion planning," *IEEE Robotics and Automation Letters*, vol. 6, no. 2, pp. 3553–3560, 2021.

[18] N. E. Ocer, G. Kaplan, F. Erdem, D. K. Matci, and U. Avdan, "Tree extraction from multi-scale uav images using mask r-cnn with fpn," *Remote Sensing Letters*, vol. 11, no. 9, pp. 847–856, 2020.

[19] J. Rückin, F. Magistri, C. Stachniss, and M. Popović, "Semi-Supervised Active Learning for Semantic Segmentation in Unknown Environments Using Informative Path Planning," *IEEE Robotics and Automation Letters*, vol. 9, no. 3, pp. 2662–2669, 2024.

[20] Y. Hao, H. Pei, Y. Lyu, Z. Yuan, J.-R. Rizzo, Y. Wang, and Y. Fang, "Understanding the impact of image quality and distance of objects to object detection performance," in *2023 IEEE/RSJ International Conference on Intelligent Robots and Systems (IROS)*, 2023, pp. 11 436–11 442.

[21] L. Qingqing, J. Taipalmaa, J. P. Queralta, T. N. Gia, M. Gabbouj, H. Tenhunen, J. Raitoharju, and T. Westerlund, "Towards active vision with uavs in marine search and rescue: Analyzing human detection at variable altitudes," in *2020 IEEE International Symposium on Safety, Security, and Rescue Robotics (SSRR)*, 2020, pp. 65–70.

[22] H. Zhu, J. J. Chung, N. R. Lawrance, R. Siegwart, and J. Alonso-Mora, "Online informative path planning for active information gathering of a 3d surface," in *2021 IEEE International Conference on Robotics and Automation (ICRA)*, 2021, pp. 1488–1494.

[23] J. Ott, E. Balaban, and M. J. Kochenderfer, "Sequential bayesian optimization for adaptive informative path planning with multimodal sensing," in *2023 IEEE International Conference on Robotics and Automation (ICRA)*, 2023, pp. 7894–7901.

[24] G. Hitz, E. Galceran, M. Garneau, F. Pomerleau, and R. Siegwart, "Adaptive continuous-space informative path planning for online environmental monitoring," *Journal of Field Robotics*, vol. 34, no. 8, pp. 1427–1449, 2017.

[25] M. Theile, H. Bayerlein, R. Nai, D. Gesbert, and M. Caccamo, "Uav path planning using global and local map information with deep reinforcement learning," in *2021 20th International Conference on Advanced Robotics (ICAR)*, 2021, pp. 539–546.

[26] J. Rückin, L. Jin, and M. Popović', "Adaptive informative path planning using deep reinforcement learning for uav-based active sensing," in *2022 International Conference on Robotics and Automation (ICRA)*, 2022, pp. 4473–4479.

[27] C. Carbone, D. Albani, F. Magistri, D. Ognibene, C. Stachniss, G. Kootstra, D. Nardi, and V. Trianni, "Distributed Autonomous Robotic Systems, 15th International Symposium," in *Distributed Autonomous Robotic Systems (DARS 2021)*, ser. Springer Proceedings in Advanced Robotics, vol. 22, 2022, pp. 306–319.

[28] A. Puente-Castro, D. Rivero, A. Pazos, and E. Fernandez-Blanco, "UAV swarm path planning with reinforcement learning for field prospecting," *Applied Intelligence*, vol. 52, no. 12, pp. 14 101–14 118, 2022.

[29] R. Ghods, W. J. Durkin, and J. Schneider, "Multi-Agent Active Search using Realistic Depth-Aware Noise Model," in *2021 IEEE International Conference on Robotics and Automation (ICRA)*, 2021, pp. 9101–9108.

[30] J. Pearl, "Reverend bayes on inference engines: a distributed hierarchical approach," in *Proceedings of the Second AAAI Conference on Artificial Intelligence*, ser. AAAI'82. AAAI Press, 1982, p. 133–136.